

# Systematic Analysis of Convection for OTREC and PREDICT

Zeljka Fuchs-Stone<sup>1</sup>, Stipo Sentic<sup>2</sup>, David J. Raymond<sup>1</sup>, and Peter Bechtold<sup>3</sup>

<sup>1</sup>New Mexico Tech

<sup>2</sup>New Mexico Institute of Mining and Technology

<sup>3</sup>European Center for Medium range Weather Forecast, UK

November 22, 2022

## Abstract

The systematic analysis of convection and the environment is performed for two field projects, OTREC and PREDICT by implementing 3DVAR on drosondes data sets. Vertically integrated moisture convergence is taken to be a proxy for convection. The interplay between the thermodynamic parameters is examined for three different stages of convection: strong convection, medium to weak and weak to null convection. It is found that for strong convection saturation fraction anti-correlates with instability index and DCIN in a similar manner for all analyzed regions of PREDICT and OTREC, while the differences in the environment become more pronounced as we move towards weak and null convection. ECMWF operational model is used to look at the time evolution of convection. As convection increases, saturation fraction increases while instability index and DCIN decrease. The boundary layer and free troposphere both play an important role in convection development in OTREC and PREDICT regions.

1                   **Systematic Analysis of Convection for OTREC and PREDICT**  
2

3                   **Ž. Fuchs-Stone<sup>1,2</sup>, S. Sentić<sup>1</sup>, D. J. Raymond<sup>1,2</sup>, and P. Bechtold<sup>3</sup>**

4                   <sup>1</sup>Climate and Water Consortium, New Mexico Tech, 801 Leroy Place, Socorro, NM.

5                   <sup>2</sup>Physics Department, New Mexico Tech, 801 Leroy Place, Socorro, NM.

6                   <sup>3</sup>European Centre for Medium-Range Weather Forecasts, Shinfield Park, Reading, United  
7 Kingdom

8  
9 Corresponding author: Željka Fuchs-Stone ([zeljka.fuchs@nmt.edu](mailto:zeljka.fuchs@nmt.edu))  
10

11                   **Key points:**

- 12                   • Both boundary layer (DCIN) and free troposphere (saturation fraction and instability index)  
13                   are very important for development of convection.  
14                   • Strong convection correlates with saturation fraction and anti-correlates with instability  
15                   index and DCIN in a similar manner regardless of the environment.  
16                   • Weak and null convection shows a variety of behavior in different environments.

## 17 **Abstract**

18 The systematic analysis of convection and the environment is performed for two field projects,  
19 OTREC and PREDICT by implementing 3DVAR on drospondes data sets.

20 Vertically integrated moisture convergence is taken to be a proxy for convection. The interplay  
21 between the thermodynamic parameters is examined for three different stages of convection:  
22 strong convection, medium to weak and weak to null convection. It is found that for strong  
23 convection saturation fraction anti-correlates with instability index and DCIN in a similar manner  
24 for all analyzed regions of PREDICT and OTREC, while the differences in the environment  
25 become more pronounced as we move towards weak and null convection.

26 ECMWF operational model is used to look at the time evolution of convection. As convection  
27 increases, saturation fraction increases while instability index and DCIN decrease.

28 The boundary layer and free troposphere both play an important role in convection development  
29 in OTREC and PREDICT regions.

30

## 31 **Plain Language Summary**

32 Convection in the tropics is the main mechanism that brings bad weather, storms and hurricanes.  
33 Understanding how convection develops and what it depends on is a question that we have been  
34 trying to answer for many decades. The characteristics of the environment can help in this task.  
35 The data from two field projects, OTREC2019 and PREDICT2010 are analyzed here to show what  
36 characteristics of the environment we should pay attention to. This can help us in improving the  
37 weather models and forecast.

38

## 39 **1. Introduction**

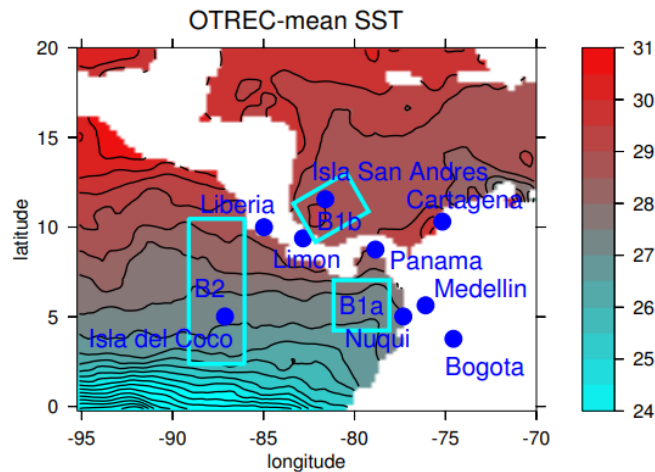
40 Mesoscale convective systems (MCS) are responsible for most rain in the tropics, Houze (1989).  
41 They are ensembles of convection that one can regard as entraining plumes of 1 - 5 km diameter  
42 that go through their life cycle almost independently of one another. If the convection grows in  
43 time that implies that the number of plumes is getting larger and the area of convection covers a  
44 larger area, while when convection decays, their number is getting smaller. This school of thought  
45 studies the evolution, i.e. growth and decay of MCSs as well as their detailed structure (Arakawa  
46 and Shubert 1974; Zipser, 1969, 1977; Houze, 1989, 2004; etc.; personal communication with Ed  
47 Zipser).

48 Another school of thought tries to study the broader properties of MCSs and most importantly their  
49 interaction with the environment, Raymond et al. (2011). This approach does not look at the  
50 individual structure of the MCSs, but how the environment governs their overall characteristics.  
51 The goal is to identify the thermodynamic properties of the environment that lead to MCSs. If one  
52 gets those right, it would be possible to correctly parametrize convection, Raymond and Fuchs-  
53 Stone (2020).

54 What properties of the environment guide convection? Is it the boundary layer, free troposphere  
55 or both? There are many papers that suggest that the boundary layer is responsible for the

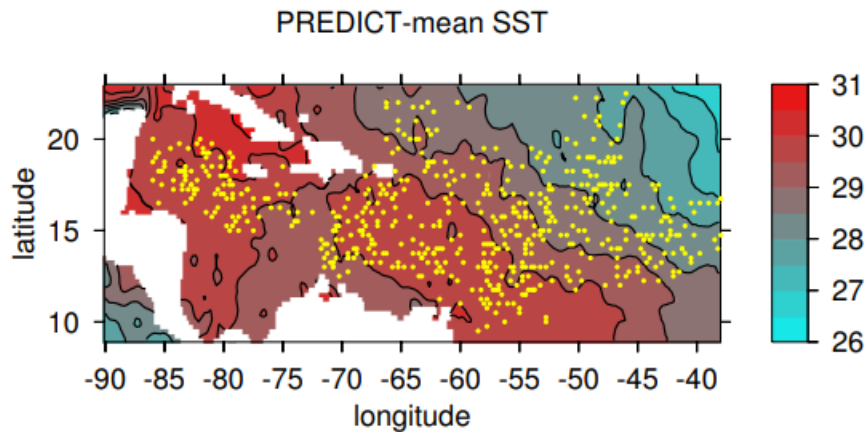
56 intertropical convergence zone, ITCZ (Riehl et al., 1951; Lindzen and Nigam, 1987; Battisti et al.,  
57 1999; Tomas et al., 1999; Stevens et al., 2002). Back and Bretherton (2009) postulate two types of  
58 convection, one that is generated by the boundary layer convergence and another that is generated  
59 by free troposphere noting that the boundary layer convergence is of more importance in east and  
60 central Pacific ITCZ. Raymond (2017) advocates for the importance of thermodynamic factors  
61 mainly in the free troposphere.

62 In this paper, we aim to systematically look at the data from the field projects OTREC and  
63 PREDICT as together they provide a data set for a wide range of sea surface temperatures (SST),  
64 298 to 304 K, in the tropics. Figure 1 shows the OTREC flight locations and SST, while Figure 2  
65 shows the same for PREDICT.



66  
67 **Figure 1:** OTREC flight area given by blue boxes and NOAA AVHRR SST averaged over the  
68 project period (Raymond and Fuchs, 2020).

69 OTREC2019 (Organization of Tropical East Pacific Convection), Fuchs-Stone et al. (2020),  
70 studied all phases of convection over the East Pacific and Southwest Caribbean from Liberia, Costa  
71 Rica using the NSF/NCAR Gulfstream V aircraft. 22 research missions were flown and 648  
72 dropsondes were successfully deployed in a grid for flight boxes B1a, the Colombian box; B1b,  
73 the Caribbean box; and B2, the Eastern Pacific ITCZ box.



74  
 75 **Figure 2:** Flight area and SST (NOAA AVHRR) during PREDICT. Yellow dots are representative  
 76 of locations where dropsondes were deployed (Raymond and Fuchs, 2020).

77  
 78  
 79 PREDICT2010 (Pre-Depression Investigation of Cloud-Systems in the Tropics), Montgomery et  
 80 al. (2012), studied systems with potential to develop into tropical cyclones in the Western Atlantic  
 81 and Caribbean using the NSF/NCAR Gulfstream V aircraft. 26 research missions were flown and  
 82 547 dropsondes were deployed.

83 Our results are based primarily on dropsonde data on which three-dimensional variational analysis  
 84 (3DVAR) is performed to obtain regular grids of data 0.25 by 0.25 degree (Lopez and Raymond,  
 85 2011; Raymond and Lopez, 2011; Raymond et al., 2011; Montgomery et al., 2012; Gjorgjievska  
 86 and Raymond, 2014; Juracic and Raymond, 2016; Fuchs-Stone et al., 2020; Raymond and Fuchs-  
 87 Stone, 2020). The data set for dropsondes used in this paper is NCAR/EOL AVAPS Dropsonde  
 88 Quality Controlled Data Version 1.0, Voemel, H. (2019).

89 Section 2 defines the thermodynamic parameters used to analyze convection from OTREC and  
 90 PREDICT, section 3 presents the results and their interpretation, while conclusions are given in  
 91 section 4.

92  
 93 **2. Thermodynamic parameters**

94 The chosen proxy for convection is vertically integrated moisture convergence that is defined as:

$$MC = - \int \nabla \cdot (\rho \mathbf{v} r)$$

96 where  $\rho$  is the density,  $\mathbf{v}$  is the horizontal components of velocity and  $r$  is the mixing ratio.

97 The thermodynamic parameters shown to be of most importance (Raymond and Fuchs, 2020) that  
 98 will be analyzed and compared to moisture convergence, i.e. convection, are saturation fraction,  
 99 instability index and deep convective inhibition.

100 The saturation fraction is defined as precipitable water over the saturated precipitable water

$$101 \quad SF = \frac{\int r dp}{\int r_s dp}$$

102 where  $r_s$  is the saturation mixing ratio and  $p$  is the pressure. It is a measure for column relative  
103 humidity.

104 The instability index is defined as:

$$105 \quad II = s_{low} - s_{high}$$

106 where  $s_{low}$  is the saturated moist entropy averaged over the altitude ranges of 1-3 km while  $s_{high}$   
107 is averaged over 5-7 km. The instability index is a measure of low to mid-tropospheric moist  
108 convective instability. Lower, but still positive, values are associated with higher saturation  
109 fraction and more rainfall (Raymond et al., 2014, Gjorgjievska and Raymond, 2014, Raymond et  
110 al., 2015, Sentic et al., 2015, Raymond and Flores, 2016, Singh et al., 2019, Raymond and Kilroy,  
111 2019). Moisture quasi-equilibrium theory postulates that the instability index is inversely  
112 proportional to saturation fraction, Raymond et al. (2014).

113 Deep convective inhibition (DCIN) is defined as

$$114 \quad DCIN = s_{th}^* - s_{bl}$$

115 where  $s_{th}^*$ , the threshold entropy, is the average of the saturated moist entropy in the 1.5 - 2 km  
116 layer and  $s_{bl}$  is the boundary layer moist entropy averaged over the 0 - 1 km layer.

117 We will also look at the difference between mass flux profiles defined as:

$$118 \quad \Delta MF = mfluxhigh - mfluxlow$$

119 where  $mfluxhigh$  is the vertical mass flux averaged over 7 – 9 km and  $mfluxlow$  over 3 – 5 km.  
120 The vertical mass flux profile is defined as the horizontally averaged product of density and  
121 vertical speed  $w$ :

$$122 \quad M(z) = \overline{\rho w}.$$

123  $\Delta MF$  is a measure of top-heaviness of convection, if it is positive the convection is more top heavy,  
124 while if it is negative it is more bottom heavy.

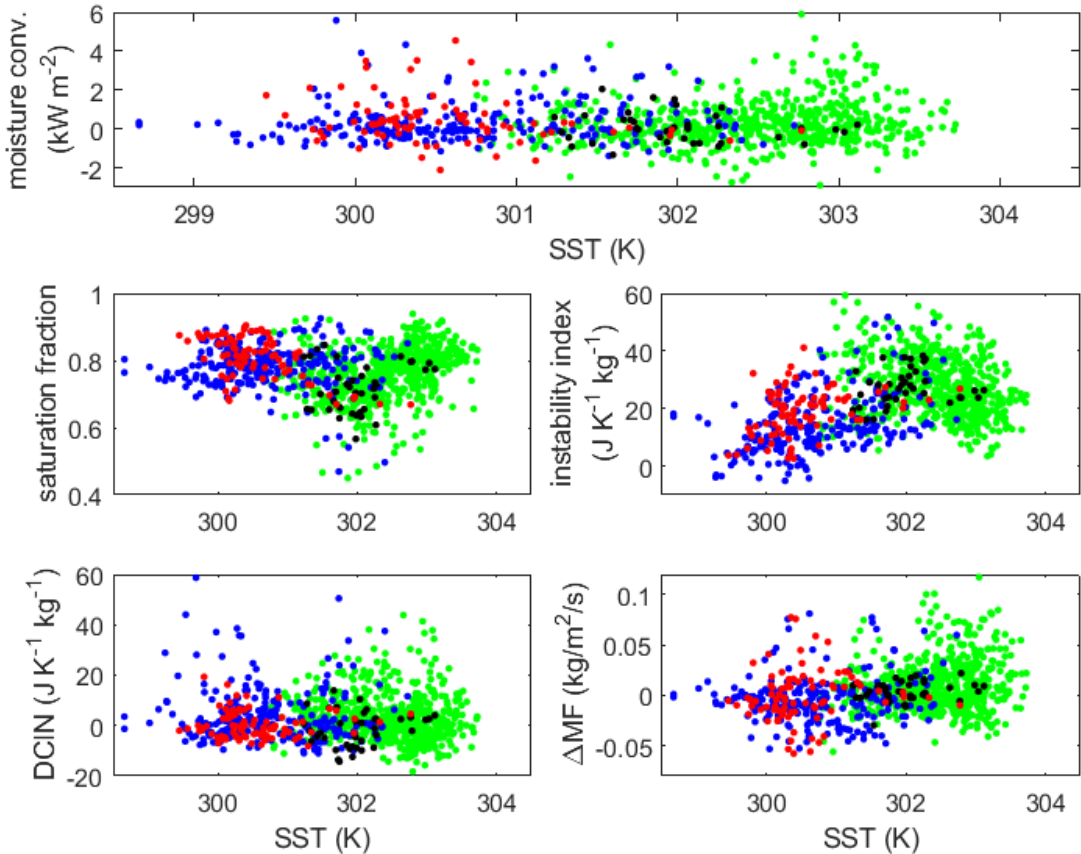
### 125 3. Results

126

#### 127 3.1 Convection and thermodynamic parameters as a function of SST

128 To systematically analyze the dropsonde data from field projects OTREC and PREDICT at the  
129 wide range of SSTs, we first analyze how moisture convergence, a proxy for convection, the  
130 thermodynamic parameters and mass flux difference  $\Delta MF$  relate to SST. Figure 3 thus shows  
131 moisture convergence, saturation fraction, instability index, DCIN and  $\Delta MF$  as a function of SST.  
132 Each dot represents the average in a one by one degree box obtained from the 3DVAR. PREDICT

133 data is shown in green, the data for the Eastern Pacific ITCZ box B2 in blue, the Pacific box off  
 134 the coast of Colombia, B1a, data is shown in red and the data for the Caribbean B1b box is shown  
 135 in black. There is an overlap between PREDICT data, B1b data and north B2 data due to higher  
 136 SSTs as well as between the south part of B2 and B1a at the lower SSTs.



137  
 138 **Figure 3:** Dependence of moisture convergence, saturation fraction, instability index, DCIN and  
 139  $\Delta MF$  on SST for OTREC and PREDICT. Green dots are PREDICT data, blue Eastern Pacific  
 140 ITCZ, red Colombian box and black Caribbean box.

141 From Figure 3, we see that moisture convergence is independent of SST. Strong convection can  
 142 occur at any values of shown SSTs except perhaps for its lowest values (299 K). This agrees with  
 143 the fact that during OTREC, we observed only one convective event in the southern part of B2 box  
 144 at 4 N latitude, Fuchs-Stone et al. (2020). It is interesting to note that although OTREC looked at  
 145 all scenarios of convection including the null one, while PREDICT targeted tropical storm  
 146 development, moisture convergence exhibits wide ranges of values in both data sets. In other  
 147 words, both OTREC and PREDICT data show strong, medium, weak and null convection.

148 Looking at the saturation fraction dependence on SST, we see a uniform spread, i.e. there is no  
 149 dependence of saturation fraction on SST except perhaps for PREDICT data that also shows lower

150 values of saturation fraction. This might be due to the particular nature of the PREDICT domain.  
151 Those lower values of saturation fraction are not associated with deep convection.

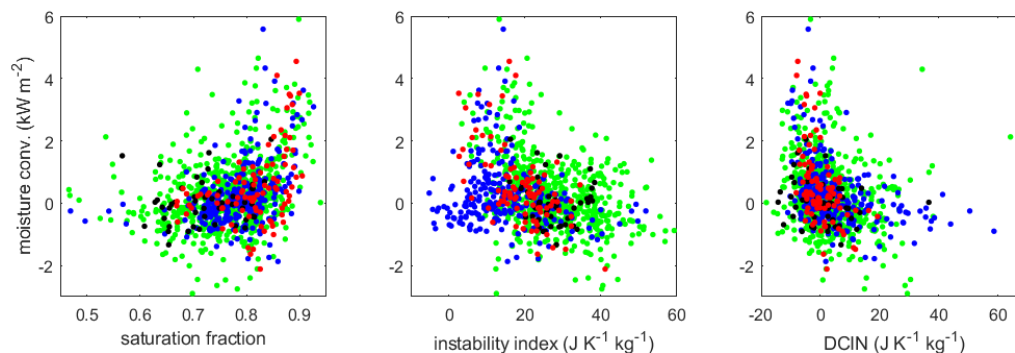
152 The instability index as shown in Figure 3 is clearly a function of SST with higher SSTs  
153 corresponding to larger values of the instability index. This comes as no surprise as the instability  
154 index is defined by using the saturated moist entropy, i.e. the temperature just above the boundary  
155 layer. Note that in the regions of large mid-level vorticity it is possible to have low instability index  
156 regardless of SST, Raymond et al. (2014).

157 DCIN appears to be independent of SST. Unlike the instability index and saturation fraction that  
158 mostly describe the free or full troposphere, DCIN describes the boundary layer. Low and negative  
159 DCIN mean that there is no inversion or inversion is weak and convection is free to develop. The  
160 high values of DCIN at the low values of SST seen by blue dots in Figure 3 show the area in south  
161 part of B2 with inversion.

162 Mass flux difference  $\Delta MF$ , that is the measure for top-heaviness of convection, has higher and  
163 positive values for higher SSTs, while it is negative for lower SSTs. This implies that at lower  
164 SSTs we have prevailing bottom heavy convection, while for higher SSTs it is mostly top heavy.  
165 Similar result was obtained by Raymond and Fuchs (2020) shown in their Figure 11.

166 To summarize the findings from Figure 3, lower SST is associated with lower values of instability  
167 index and bottom heavy vertical mass flux profile while higher SST is associated with higher  
168 values of instability index and top heavy vertical mass flux profile. DCIN, saturation fraction and  
169 moisture convergence do not depend on SST.

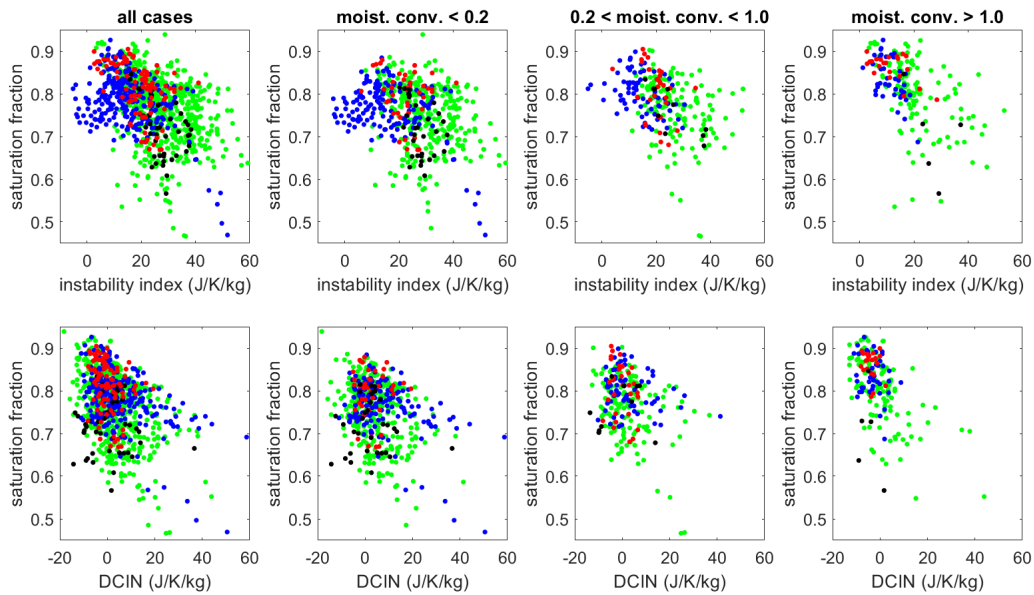
### 170 3.2 The interplay between convection and thermodynamic parameters



171  
172 **Figure 4:** Scatter plot of moisture convergence and saturation fraction, instability index and DCIN.  
173 Green dots are PREDICT data, blue Eastern Pacific ITCZ, red Colombian box and black Caribbean  
174 box.

175  
176 Figure 4 shows how our thermodynamic parameters saturation fraction, instability index and DCIN  
177 correlate with moisture convergence, i.e. convection. We see that higher values of saturation  
178 fraction lead to more convection. The opposite is true for the instability index where lower values

179 correspond to more convection. Similarly to the instability index, but perhaps even more  
 180 pronounced, negative and small values of DCIN lead to more convection.



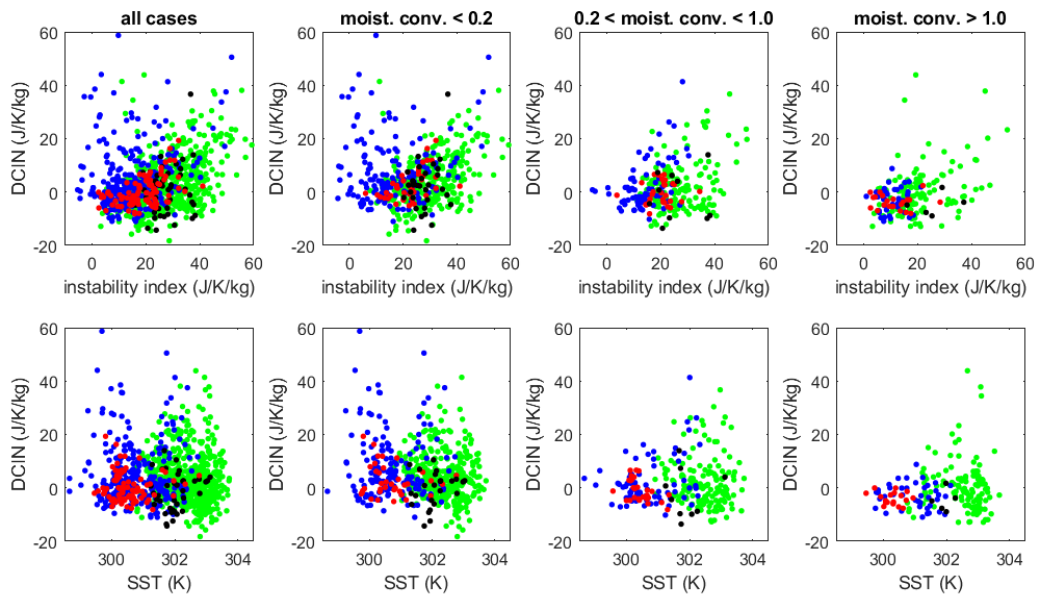
181

182 **Figure 5:** Scatter plots between saturation fraction and instability index (top panel) and saturation  
 183 fraction and DCIN (bottom panel) for all cases, null to weak convection, weak to medium  
 184 convection and strong convection.

185 To decipher Figure 4, that includes all cases from null to strong convection, we now set out to look  
 186 at the relationships between our thermodynamic parameters saturation fraction, instability index  
 187 and DCIN for different phases of convection. We define convection by the strength of vertically  
 188 integrated moisture convergence. If moisture convergence is greater than  $1 \text{ kWm}^{-2}$  we define it  
 189 as strong convection, if it is between  $0.2$  and  $1 \text{ kWm}^{-2}$  weak to medium convection and if it is  
 190 less than  $0.2 \text{ kWm}^{-2}$  weak to null convection.

191 Figure 5 shows scatter plots between saturation fraction and instability index (top panel) and  
 192 saturation fraction and DCIN (bottom panel) for, starting from the left in the figure, all cases, null  
 193 to weak convection, weak to medium convection and strong convection cases. For strong  
 194 convective cases the saturation fraction and instability index show a clear anti-correlation as per  
 195 moisture quasi-equilibrium theory. The scatter plot between saturation fraction and DCIN shows  
 196 without a doubt that negative or very small DCIN is required for strong convection. The scatter  
 197 plot for weak to medium convection tells a similar story, but with more scattering. As expected  
 198 the saturation fraction can be lower and instability index and DCIN higher. For weak to null  
 199 convection, the scattering is even wider in both saturation fraction vs instability index and  
 200 saturation fraction vs DCIN. This is to be expected as when there is weak or null convection the  
 201 moisture quasi-equilibrium theory does not hold as the environment is too dry and DCIN naturally  
 202 turns towards higher positive values. However, it is interesting to note some differences between  
 203 the sets of data. The Eastern Pacific ITCZ box B2, even in weak to null cases, shows high

204 saturation fraction values and low instability index, while we don't see the same in other regions.  
205 The scattering is more pronounced for PREDICT and B2 data than for others.



206

207 **Figure 6:** Scatter plots between DCIN and instability index (top panel) and DCIN and SST (bottom  
208 panel) for all cases, null to weak convection, weak to medium convection and strong convection.

209 Lastly, let's look at the relationship between DCIN and instability index and DCIN and SST for  
210 different phases of convection. Figure 6 shows the scatter plots between DCIN and instability  
211 index (top panel) and DCIN and SST (bottom panel). In a regime of strong convection, small DCIN  
212 corresponds to small instability index. Similar is true for weak to medium convection except that  
213 there is more scattering. In a regime of null to weak convection the scattering is even more  
214 pronounced with the possibility of high values of DCIN and low values of instability index in the  
215 B2 data. Looking at the bottom panel, we can see that those cases correspond to the ones at the  
216 southern part of the B2 box where inversion is present, also seen in EPIC2001 (East Pacific  
217 Investigation of Climate) data, Raymond (2017). For weak to medium convection as well as for  
218 strong convection, there is no dependence of DCIN on SST.

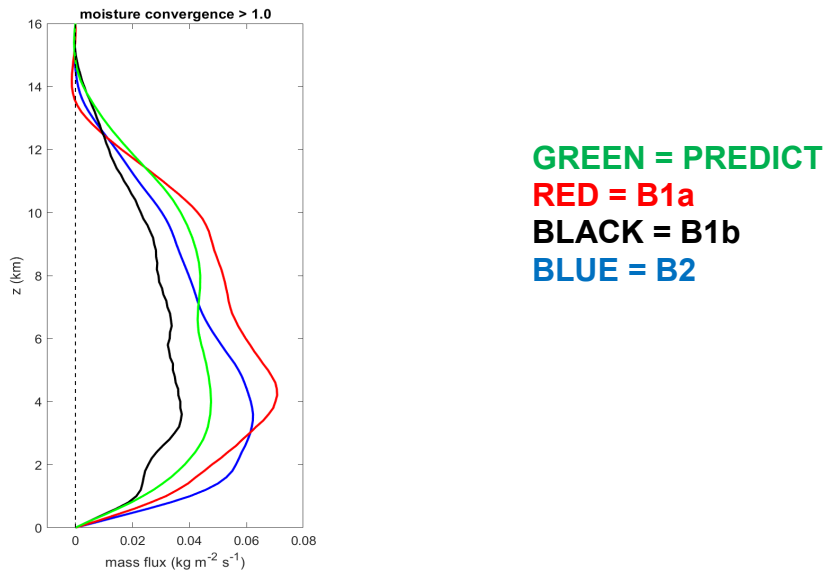
219 Figures 3 – 6 tell an interesting story. Strong convection seems to be similar in all regions, no  
220 matter what the SST is, whether we are close to land or not, once there is significant convection,  
221 there is no doubt that moisture convergence depends on high saturation fraction, low instability  
222 index and low DCIN. Furthermore, saturation fraction anti-correlates with instability index and  
223 DCIN in a similar manner. When convection is weak and the environment is dry, the time scale  
224 for convection to adjust the moisture to the equilibrium value for a given value of instability index  
225 is long and this anti-correlation is not necessarily observed. DCIN takes up higher values indicating  
226 inversion. The differences between observed regions are more apparent in the cases of null to weak  
227 convection and this is a subject for future research.

228

229

### 230 3.3 Vertical mass flux profiles

231 Differences in vertical mass flux profiles could indicate differences between convection in  
232 different regions. Figure 7 shows the average vertical mass flux profiles for strong convection  
233 when moisture convergence is greater than  $1 \text{ kWm}^{-2}$  for 3 OTREC regions as well as for  
234 PREDICT.



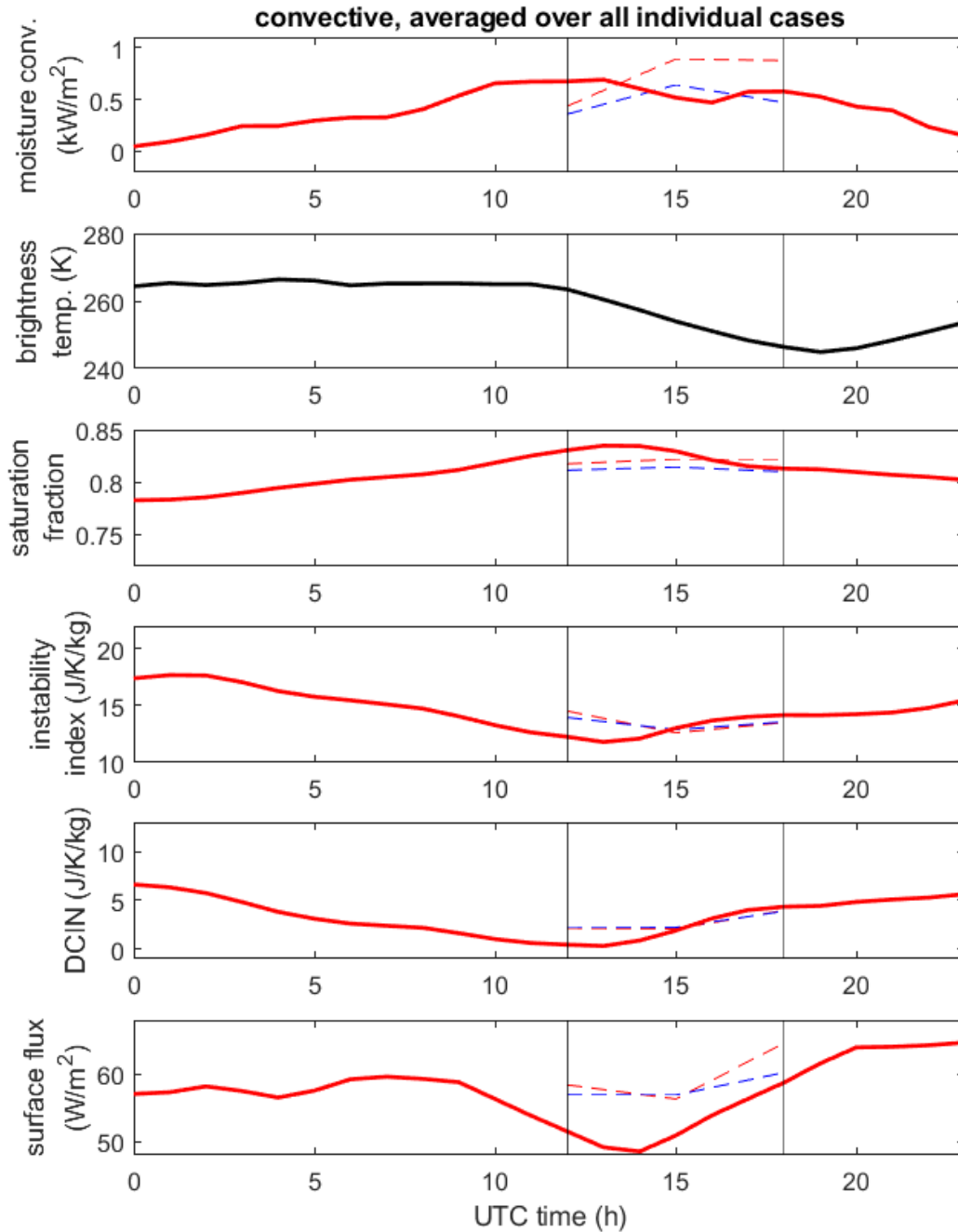
235

236 **Figure 7:** Averaged vertical mass flux profiles for PREDICT and OTREC for strong convection

237 From Figure 7 we can see that on average all vertical mass flux profiles in strong convection show  
238 deep vertical mass flux profiles. The profiles for PREDICT and the Caribbean B1b box are similar,  
239 with higher values in PREDICT. This might be because during OTREC we weren't able to fly into  
240 many strong convective cases in B1b, in fact, there were only 3 and they were not too strong,  
241 Fuchs-Stone et al. (2020). The vertical mass flux profiles for the Eastern Pacific ITCZ box B2 and  
242 the Colombian box B1a have even higher values than PREDICT and B1b. The mass flux profile  
243 in B1a box is more top-heavy than the one in B2 box.

### 244 3.4 Time evolution

245 To look at the time evolution of the convective cases, we first use the 3DVAR data from OTREC  
246 to define convective one by one degree box averages, defined as boxes with moisture convergence  
247 greater than  $1 \text{ kWm}^{-2}$ . We then average the European Centre for Medium-Range Weather  
248 Forecasts (ECMWF) operational model data in boxes with the same longitude and latitude for all  
249 times of the same day. Then we average all the hourly values. The same method is applied to the  
250 Geostationary Operational Environmental Satellite (GOES-16) brightness temperature. The results  
251 are shown in Figure 8.



252

253 **Figure 8:** Moisture convergence, GOES-16 brightness temperature, saturation fraction, instability  
 254 index, DCIN and surface latent heat fluxes averaged over all strong convective cases from OTREC.  
 255 Solid red line represents ECMWF operational model results, solid black line GOES-16 results,  
 256 while red and blue dashed lines show results from operational ECMWF model with and without  
 257 dropsondes assimilated respectively.

258 Figure 8 shows moisture convergence, brightness temperature from the GOES-16, saturation  
259 fraction, instability index, DCIN and surface latent heat fluxes averaged over all strong convective  
260 cases from OTREC as a function of time. The vertical lines bound the time of a day when OTREC  
261 dropsondes were deployed and assimilated into the EC model (12 to 18 UTC). The red solid line  
262 shows the results from the ECMWF operational model.

263 We can see that the convection represented by moisture convergence peaks between 10 and 13  
264 hours UTC, 4 to 7 am local time. This agrees with our observations while in the field. On average  
265 convection was developing in the very early morning hours, becoming stratiform around 10 am  
266 local time, 16 UTC. The black solid line in the second panel represents the brightness temperature  
267 from satellite observations GOES-16 for the same convective cases. Its minimum lags the  
268 maximum of the moisture convergence from the EC model due to the lag between convection and  
269 resulting stratiform cloudiness as the upper troposphere needs time to become optically thick,  
270 Bechtold et al. (2014). This gives us confidence in EC model of moisture convergence evolution  
271 as of the other parameters.

272 The red and the blue dashed lines represent the results from the EC operational model ran for 6  
273 hours when our research flights took place. The intention is to compare the model with and without  
274 dropsondes to gain more confidence in the results of the model outside of that timeline. The run in  
275 which dropsonde data were assimilated is shown in red dashed line, while the one without the  
276 dropsondes assimilated is shown in blue dashed line. We can see that the model does very well  
277 when it calculates saturation fraction, instability index, DCIN and to some degree surface fluxes  
278 regardless to dropsondes being assimilated. The biggest difference is seen in the moisture  
279 convergence. The model underestimates moisture convergence when the dropsondes are not  
280 assimilated. This is why we looked at the GOES-16 brightness temperature as well.

281 We now look at the time evolution for moisture convergence, saturation fraction, instability index,  
282 DCIN and surface latent heat fluxes (Yu and Weller, 2008), from the EC model represented by red  
283 solid line. Prior to the peak in the moisture convergence saturation fraction increases while the  
284 instability index and DCIN decrease. They reach their maximum (saturation fraction) and minima  
285 (instability index and DCIN) at the same time, a bit after the maximum in moisture convergence.  
286 The reason behind this lag might be that sacrificial convection seen by moisture convergence has  
287 to first moisten the environment as per moisture quasi-equilibrium theory. The surface latent heat  
288 fluxes, Yu and Weller (2008), shown in bottom panel of Figure 8 decrease prior to convection due  
289 to a decrease in the surface wind speed.

#### 290 **4. Conclusions**

291 The goal of this study is to systematically look at the 3DVAR analysis from the dropsonde data  
292 for the field projects OTREC and PREDICT to see how convection behaves in different  
293 environments and if the convection is different depending on its strength. Some of the questions  
294 that we try to answer are: Does convection change with different SSTs and is it different if there  
295 is proximity to land? Is convection different if it is strong, medium or weak in different  
296 environments? OTREC data covers 3 diverse environments. The research flight area in the Eastern  
297 Pacific ITCZ, B2, covers the region with strong meridional sea surface temperature gradients,

298 while B1b, the Caribbean region, covers the area with uniform and high SSTs. B1a box just off  
299 the coast of Colombia covers the environment of lower SSTs in the proximity of land. The  
300 PREDICT data covers a vast region of the western Atlantic and Caribbean, a region with high  
301 SSTs and higher latitudes than OTREC.

302 We take vertically integrated moisture convergence as a proxy for convection. The thermodynamic  
303 parameters used to describe convection are saturation fraction, instability index and DCIN. We  
304 first look at the dependence of convection, thermodynamic parameters and mass flux difference  
305 on SST to get a general picture. We see that deep convection can occur at any observed SST higher  
306 than 299.5 K which corresponds to well-known 26.5 C threshold for development of tropical  
307 disturbances and deep convection, Palmen (1948) and Grey (1968). Convection, saturation fraction  
308 and DCIN do not depend on SST, while instability index and mass flux difference do. Lower SST  
309 regions have smaller instability index and more bottom heavy vertical mass flux while higher SST  
310 regions have larger instability index and more top heavy convection.

311 Classifying convection into strong, medium, and weak to null and looking at the interplay of  
312 convection and thermodynamic parameters within those limits tells an interesting story. Strong  
313 convection looks very similar regardless to the environment, SST, proximity to land, different  
314 latitude etc. Moisture convergence, i.e. convection is strongly correlated with saturation fraction  
315 and anti-correlated with instability index and DCIN. Furthermore, saturation fraction shows  
316 similar anti-correlation with instability index and DCIN for every region that we have looked at.  
317 This implies that both, the boundary layer (DCIN) and free troposphere (saturation fraction and  
318 instability index) are very important for development of convection.

319 As we move towards medium and weak to null convection, the story becomes more complicated.  
320 The above correlations are less pronounced and more scattered. When there is no convection or  
321 convection is very weak, the environment looks different depending on the area we look at and  
322 those regional differences are left for future research.

323 The time evolution of moisture convergence, thermodynamic parameters and surface fluxes is  
324 analyzed using the ECMWF operational model for the events with strong convection during  
325 OTREC. Before the peak of convection saturation fraction increases and instability index and  
326 DCIN decrease. Maxima and minima of saturation fraction, instability index and DCIN are reached  
327 simultaneously. The surface latent heat fluxes decrease prior to convection. The significance of  
328 the impact of surface fluxes is not certain and is left for future research.

329 It is important to note that we are looking at convection and the environment rather than the  
330 evolution of individual plumes. Such analysis gives broad statistical answers and could help  
331 improve cumulus parametrizations, Raymond and Fuchs-Stone (2020).

332

333 **Acknowledgments**

334  
335 We would like to acknowledge operational, technical and scientific support provided by NCAR's  
336 Earth Observing Laboratory, sponsored by the National Science Foundation. The NCAR/EOL  
337 AVAPS Dropsonde QC Data DOI: <https://doi.org/10.26023/EHRT-TN96-9W04>. Data is  
338 provided by NCAR/EOL under the sponsorship of the National Science  
339 Foundation <https://data.eol.ucar.edu/>. We thank students Katie Jensen and Marc Gross for their  
340 work on GOES-16 data. This work was supported by National Science Foundation grant  
341 1758513.

342

343

344 **References**

345

346 Arakawa, A. and W. H. Schubert, (1974), Interaction of a cumulus cloud ensemble with the large-  
347 scale environment, Part I. *J. Atmos. Sci.*, 31, 674-701.

348

349 Back, L. E., and C. S. Bretherton, (2009), On the relationship between SST gradients, boundary  
350 layer winds, and convergence over the tropical oceans, *J. Climate*, 33, 4182-4196.

351

352 Battisti, D. S., E. S. Sarachik, and A. C. Hirst, (1999), A consistent model for the large-scale steady  
353 surface atmospheric circulation in the tropics, *J. Climate*, 12, 2956-2964.

354

355 Bechtold, P., N. Semane, P. Lopez, J. Chaboureau, A. Beljaars, and N. Bormann, 2014:  
356 Representing Equilibrium and Nonequilibrium Convection in Large-Scale Models. *J. Atmos.*  
357 *Sci.*, **71**, 734–753, <https://doi.org/10.1175/JAS-D-13-0163.1>.

358

359 Emanuel, K., 2020, Slow modes of the equatorial waveguide. *J. Atmos. Sci.*, **77**, 1575-1582,  
360 doi:10.1175/jas-d-19-0281.1.

361

362 Fuchs, Ž. and Raymond, D. J, (2017), A simple model of intraseasonal oscillations, *J. Adv. Model.*  
*Earth Syst.*, 9, 1195– 1211, doi:[10.1002/2017MS000963](https://doi.org/10.1002/2017MS000963).

363

364 Fuchs-Stone, Z., D. J. Raymond and S. Sentic, (2020), OTREC2019: Convection over the East  
Pacific and Southwest Caribbean. *Geophys. Res. Lett.*, 47, doi:10.1029/2020GL087564.

365

366 Gjorgjievska, S. and D. J. Raymond, (2014), Interaction between dynamics and thermodynamics  
during tropical cyclogenesis, *Atmos. Chem. Phys.*, 14, 3065-3082.

367

368 Gray, W. M., (1968), Global view of the origin of tropical disturbances and storms, *Mon. Wea.*  
*Rev.*, **96**, 669–700,

369

[https://doi.org/10.1175/1520-0493\(1968\)096<0669:GVOTOO>2.0.CO;2](https://doi.org/10.1175/1520-0493(1968)096<0669:GVOTOO>2.0.CO;2).

370

371 Houze, R. A., (1989), Observed structure of mesoscale convective systems and implications for  
large-scale heating. *Quart. J. Roy. Meteor. Soc.*, 115, 425-461.

372

373 Houze, R. A., (2004), Mesoscale convective systems. *Rev. Geophys.*, 42, RG4003,  
doi:10.1029/2004RG000150.

374 Juracic, A., and D. J. Raymond, (2016), The effects of moist entropy and moisture budgets on  
375 tropical cyclone development. *J. Geophys. Res.*, 121, 9458-9473.

376 Lindzen, R. S., and S. Nigam, (1987), On the role of sea surface temperature gradients in forcing  
377 low-level winds and convergence in the tropics, *J. Atmos. Sci.*, 44, 2418-2436.  
378

379 Lopez Carrillo, C., and D. J. Raymond, (2011), Retrieval of three-dimensional wind fields from  
380 Doppler radar data using an efficient two-step approach. *Atmos. Meas. Tech.*, 4, 2717-2733,  
381 doi:10.5194/amt-4-2717-2011.

382 Montgomery, M. T., Davis, C., Dunkerton, T., Wang, Z., Velden, C., Torn, R., Majumdar, S. J.,  
383 Zhang, F., Smith, R. K., Bosart, L., Bell, M. M., Haase, J. S., Heymsfield, A., Jensen, J., Campos,  
384 T., and Boothe, M. A., (2012), The Pre-Depression Investigation of Cloudsystems in the Tropics  
385 (PREDICT) experiment, *B. Am. Meteor. Soc.*, 93, 153–172.

386 Palmen, E. H., (1948), On the Formation and Structure of Tropical Cyclones,” *Geophysica,*  
387 *Helsinki*, Vol. 3, pp. 26-38.

388 Raymond, D. J., S. L. Sessions, and C. Lopez Carrillo, (2011), Thermodynamics of tropical  
389 cyclogenesis in the northwest Pacific, *J. Geophys. Res.*, 116, D18101,  
390 doi:10.1029/2011JD015624.

391 Raymond, D. J. and C. Lopez Carrillo, (2011), The vorticity budget of developing typhoon Nuri  
392 (2008), *Atmos. Chem. Phys.*, 11, 147-163, doi:10.5194/acp-11-147-2011.

393 Raymond, D. J., S. Gjorgjievska, S. Sessions, and Z. Fuchs, (2014), Tropical cyclogenesis and  
394 mid-level vorticity. *Australian Meteorological and Oceanographic Journal*, 64, 11-25.  
395

396 Raymond, D. J., Z. Fuchs, S. Gjorgjievska and S. L. Sessions, (2015), Balanced dynamics and  
397 convection in the tropical troposphere. *J. Adv. Model. Earth Syst.*, 7, doi:10.1002/2015MS000467.  
398

399 Raymond, D. J. and M. M. Flores, (2016), Predicting convective rainfall over tropical oceans from  
400 environmental conditions. *J. Adv. Model. Earth Syst.*, 8, doi:10.1002/2015MS000595.  
401

402 Raymond, D. J., (2017), [Convection in the east Pacific intertropical convergence zone](#). *Geophys.*  
403 *Res. Lett.*, 44, 562-568, doi:10.1002/2016GL071554.  
404

405 Raymond, D. J. and G. Kilroy, (2019), Control of convection in high-resolution simulations of  
406 tropical cyclogenesis. *J. Adv. Model. Earth Syst.*, 11, 1582-1599.  
407

408 Raymond and Fuchs-Stone, (2020), Emergent Properties of Convection in OTREC and PREDICT.  
409 *Journal of Geophysical Research: Atmospheres*.  
410

411 Riehl, H., T. C. Yeh, J. S. Malkus and N. E. La Seur, (1951), The north-east trade of the Pacific  
412 ocean, *Quart. J. Roy. Meteor. Soc.*, 77, 598-626.

413 Sentić, S., Sessions, S. L., and Fuchs, Ž., (2015), Diagnosing DYNAMO convection with weak  
414 temperature gradient simulations, *J. Adv. Model. Earth Syst.*, 7, 1849– 1871,  
415 doi:[10.1002/2015MS000531](#).

416 Sentić, S., Fuchs-Stone, Ž., & Raymond, D. J, (2020), The Madden-Julian Oscillation and mean  
417 easterly winds. *Journal of Geophysical Research: Atmospheres*, 125,  
418 e2019JD030869. <https://doi.org/10.1029/2019JD030869>

419 Singh, M. S., Warren, R. A., & Jakob, C., (2019), A steady-state model for the relationship  
420 between humidity, instability, and precipitation in the tropics. *Journal of Advances in Modeling  
421 Earth Systems*, **11**, 3973– 3994. <https://doi.org/10.1029/2019MS001686>

422 Stevens, B., J. Duan, J. C. McWilliams, M. Munnich, and J. D. Neelin, (2002), Entrainment,  
423 Rayleigh friction, and boundary layer winds over the tropical Pacific, *J. Climate*, 15, 30-44.

424 Tomas, R. A., J. R. Holton, and P. J. Webster, (1999), The influence of cross-equatorial pressure  
425 gradients on the location of near-equatorial convection, *Quart. J. Roy. Meteor. Soc.*, 125, 1107-  
426 1127.

427 UCAR/NCAR - Earth Observing Laboratory, Voemel, H. 2019. NCAR/EOL AVAPS Dropsonde  
428 QC Data. Version 1.0. UCAR/NCAR - Earth Observing  
429 Laboratory. <https://doi.org/10.26023/EHRT-TN96-9W04>. Accessed 13 January 2020.

430 Yu, L., Jin, X., & Weller, R. A, (2008), Multidecade global flux datasets from the Objectively  
431 Analyzed Air-sea Fluxes (OAFlux) Project: Latent and sensible heat fluxes, ocean evaporation,  
432 and related surface meteorological variables. Woods Hole Oceanographic Institution, OAFlux  
433 Project Technical Report. OA-2008-01, 64pp. Woods Hole, Massachusetts, USA.

434 Zipser, E. J., (1969), The role of organized unsaturated convective downdrafts in the structure and  
435 rapid decay of an equatorial disturbance. *J. Appl. Meteor.*, 8, 799-814.

436 Zipser, E. J., (1977), Mesoscale and convective scale downdrafts as distinct components of squall-  
437 line structure. *Mon. Wea. Rev.*, 105, 1568-1589.